A&A 401, 985–996 (2003)
DOI: 10.1051/0004-6361:20030127

Astronomy & Astrophysics

The envelope of IRC +10216 reflecting the galactic light⋆

UBV surface brightness photometry and interpretation

N. Mauron[1], P. de Laverny[2], and B. Lopez[2]

[1] Groupe d'Astrophysique, UMR 5024 CNRS, Case CC72, Place Bataillon, 34095 Montpellier, France
e-mail: mauron@graal.univ-montp2.fr
[2] Observatoire de la Côte d'Azur, Département Fresnel, UMR 6528 CNRS, BP 4229, 06304 Nice, France
e-mail: laverny@obs-nice.fr; lopez@obs-nice.fr

Received 8 July 2002 / Accepted 27 December 2002

Abstract. We present and analyse new optical images of the dust envelope surrounding the high mass-loss carbon star IRC +10216. This envelope is seen due to external illumination by galactic light. Intensity profiles and colors of the nebula were obtained in the *UBV* bandpasses. The data are compared with the results of a radiative transfer model calculating multiple scattering of interstellar field photons by dust grains with a single radius. The data show that the observed radial shape of the nebula, especially its half maximum radius, does not depend on wavelength (within experimental errors), suggesting that grains scatter in the grey regime, and this is further supported by the plateau colors being close to those of the ISRF as given by Mattila (1980a). A grain radius of 0.16 μm with envelope parameters as proposed by Groenewegen (1997) can reproduce this achromatism of shape and color characteristics. However, there remain substantial discrepancies between model and observations concerning the absolute intensity of the nebula and its radial shape. Some of these discrepancies disappear if one adopts a small grain size (~0.05 μm), or if one assumes a lower dust mass loss rate for the outer layers ($\theta \geq 20''$, corresponding to 1000 years ago). Within the framework of our simple model, we cannot determine a "dominant" grain size. Future more sophisticated models will have to take into account grain size distribution, and also explore complicated issues like the effects of grain porosity and/or asphericity on scattering, the influence of the envelope small-scale structure on the radiative transfer, and the possibility of a field anisotropy. For the same reasons, it is not presently feasible to establish with confidence whether the interstellar radiation field in the visible is significantly different in strength at the location of IRC +10216 compared to the usually adopted one in the solar neighbourhood.

Key words. stars: AGB and post-AGB – stars: circumstellar matter – ISM: dust, extinction

1. Introduction

Stars of intermediate initial mass can have very high mass-loss rates when evolving on the asymptotic giant branch (AGB). This mass loss produces extended, dusty, optically thick envelopes that strongly mask the central star in the visible domain, possibly leaving no optical counterpart. However, these envelopes are externally illuminated by the stars of the galactic disk. If deep enough, a direct image of the envelope can show the reflection of this external photon source by circumstellar grains. Two such cases of AGB reflection nebulae are presently known. The best case is the nearby carbon star IRC +10216, with an exceptionally massive circumstellar envelope that is clearly seen in the ambient galactic light in the *B* and *V* bands (Mauron & Huggins 1999). The envelope is detected up to about 3′ from center, and appears fairly round, which is qualitatively consistent with a spherically symmetric dust shell and an isotropic galactic field (at least in *B* and *V*). There is also a central *plateau* of diameter ~20″, (i.e. no central peak), which is prominent in *B* and proves that the source of photons is not the central star. The second case is CRL 3116, another carbon AGB object at about 1 kpc from the Sun (Crabtree & Rogers 1992), but this object is much less studied than IRC +10216.

In the present paper, we follow the works of Martin & Rogers (1987, hereafter MR87) and Crabtree & Rogers (1992), and our goal is to make a quantitative investigation of these reflection nebulae in order to derive information on the interstellar radiation field (ISRF) and/or the circumstellar dust properties. Briefly, the ISRF is due to the integrated light of galactic disk stars and a diffuse galactic light component. It is an important quantity involved in many problems concerning the interstellar medium or circumstellar shells, such as grain heating, their far-infrared emission and photochemistry (e.g.,

Send offprint requests to: N. Mauron,
e-mail: nicolas.mauron@graal.univ-montp2.fr

⋆ Based on observations made with the Antu 8-m VLT (ESO; program 63I-0177A), with the Canada France Hawaii 3.6-m Telescope (CNRS, NRC, UH) and the 1.20-m telescope of Haute-Provence Observatory (CNRS).

Mathis et al. 1983; van Dishoek 1994; Glassgold 1996). The intensity of the local ISRF (measured from Earth) is relatively well known in the visible range, but the situation is more controversial in the ultraviolet, with differences between authors of at least a factor of 2 at 1500 Å (see Fig. 2 of van Dishoek 1994). Concerning the spatial ISRF variations within the solar neighbourhood, one expects rather small variations, except for peaks close to very luminous stars, especially in the far ultraviolet region (Habing 1968; Jura 1974).

Martin & Rogers (1987) found that in order to account for the V surface brightness of the IRC +10216 plateau, which was relatively faint compared to their model, a possible solution was to assume an ISRF smaller than that of Mathis et al. (1983) by a factor of ∼2.5. They suggested that a faint ISRF could be due to the height of this object above the galactic plane, which is $z = 90$ pc for an assumed distance $d = 130$ pc. However, according to Mattila (1980a), the dependance on z is predicted to be much smaller than a factor of 2, at least in the optical domain. Another indication that the ISRF may have no strong minima comes from the COBE observations of interstellar dust at high galactic latitude: the narrow range of dust temperature suggests ISRF variations smaller than 30% (Lagache et al. 1998).

Martin & Rogers also noted two other possible explanations for the low plateau V-band brightness: the first is to assume a grain albedo lower than originally adopted in their model; the second is to envisage an even smaller grain radius than assumed in their model (0.05 μm) and to increase the mass loss rate in the external layers. However more recent studies of the dust of IRC +10216 point to significantly larger grain sizes: a dominant radius of 0.16 μm is found by Groenewegen (1997, GR97 hereafter). Distribution sizes including grains as large as 0.2 or 0.4 μm are also favoured by Ivezic & Elitzur (1996) and by Skinner et al. (1998).

These considerations led us to obtain additional images of the ISRF-reflecting nebula around IRC +10216. Our goal is to reanalyse the intensity, colors, size, and shape of this nebula. In particular, this paper presents new surface brightness measurements in the three UBV bandwidths (a photometric sequence of field stars is given in Appendix A). Details about the observations and the data reduction are given in Sect. 2, and the results are presented in Sect. 3. A specific Monte-Carlo radiative transfer code was developped for this program and is described in Sect. 4, with complementary considerations in Appendix B. The data are quantitatively interpreted and discussed in Sect. 5, and a summary of this work is presented in the conclusion.

2. Observations and reductions

The first set of observations was carried out at Haute-Provence Observatory with the 1.20-m telescope, equipped at the Newtonian focus with a CCD camera for $UBVRI$ imaging. The chip is a thin back-illuminated 1024^2 Tektronix, with a read-out noise of 8.5 e^- and a gain of 3.5 e^- ADU^{-1}. This instrument provides a field of $11.7' \times 11.7'$ with a scale of 0.6845 arcsec $pixel^{-1}$. More details can be found in Ilovaisky (1997). The nights were clear but the seeing was 2″. Flat-fields were done on the dome and on the sky. The UBV images of IRC +10216 obtained are listed in Table 1. Several images were also taken each night on the calibration fields NGC 2403 (Zickgraf et al. 1990) and M 13 (Arp & Johnson 1955). All CCD frames were reduced in the standard way, with bias substraction and division by averaged flat-fields. These data permitted the establishment of a UBV photometric sequence containing 16 stars in the field of IRC +10216 (details in Appendix A).

The CFHT observations are listed in Table 1 and were described by Mauron & Huggins (1999). They resulted into two deep B and V images, with a field of $8.7' \times 8.7'$ and a scale of 0.436 arcsec $pixel^{-1}$. Because no photometric standards were observed at CFHT, calibration was achieved by considering unsaturated stars of the OHP sequence.

The VLT observations were done in service mode with the Antu 8-m telescope, equipped with the FORS1 focal reducer (Table 1). The detector is a 2048^2 thinned 24 μm pixel Tektronix chip. The field of view is $6.83' \times 6.83'$ with a pixel size of 0.200 arcsec $pixel^{-1}$. More details on the instrumentation can be found in the FORS1 Manual at ESO Web site. The usable data consists of three 8-min U frames and two 2-min V frames. A number of other frames in UBV were acquired on different nights, but had to be rejected for this study due to an excessively bright sky or poor photometric conditions. The frames were merged into one U and one V flat-fielded image (This 4 mn VLT V-band image is much less deep than the CFHT one presented in Mauron & Huggins 1999), and is not shown here; for the U-band image, see below). During the nights of observation, one or two exposures per filter were supplied of calibration fields (Mark A, SA 101 and PG 0942-029, detailed on the FORS ESO Web site). These exposures did not allow an independant determination of the atmospheric extinction coefficients of these nights, but if plausible values are assumed ($k_U = 0.62$, $k_V = 0.14$ mag/airmass), one finds that the U and V photometry of the field stars agree very well with the OHP results, with differences of 0.04 mag in V, and 0.03 mag in $U - V$. Therefore, all measurements on the nebula were calibrated using the OHP UBV sequence.

After bias subtraction and flat-field correction, our goal was to obtain surface photometry of the plateau in the UBV bands, and to derive the surface brightness profiles. The main difficulty is to estimate the background sky level to be subtracted, for several reasons. First, the plateau is intrinsically faint, about 4% of the sky brightness in V. This implies that, if an accuracy of ∼10% is desired for the plateau photometry, the sky brightness far from the nebula has to be determined with a relative error of ∼0.4%. The flat field correction should also be achieved with this accuracy over large or medium angular scales, but in practice the corrected images show small but non-negligible gradients. These gradients can be corrected in part by dividing by second order polynomial functions, but residual variations remain at intermediate scales. The situation is also complicated by the fact that there are three bright stars in the field: they produce haloes, various ghosts, and significant diffuse parasite light that is not uniform. Nevertheless, these defects depend on the intrumentation used, and we could perform cross-verifications between OHP, CFHT, and VLT data. The surface photometry of the nebula was obtained with

Table 1. Log. of observations of IRC +10216.

Telescope	Date	Band	Exposures
OHP 1.2 m	27-28 Jan. 1998	*B*	4×1 hr
OHP 1.2 m	27-28 Jan. 1998	*V*	2×1 hr
OHP 1.2 m	28-29 Jan. 1998	*U*	5×1 hr
CFH 3.6 m	17-18 Feb. 1998	*V*	4×20 mn
CFH 3.6 m	17-18 Feb. 1998	*B*	2×20 mn
VLT 8.0 m	6 Jun. and 9 May 1999	*U*	3×8 mn
VLT 8.0 m	9 May 1999	*V*	2×2 mn

azimuthally averaged radial profiles. In the *U*-band, the center position given by the *V* frames was adopted . The profiles are achieved after masking all stars, galaxies, bright stars and their haloes, and other obvious defects (see MH99 for more details).

3. Observational results

The reduction of all images resulted in the final plateau *UBV* surface photometry given in Table 2. The *UBV* measurements refer to the top of the plateau, i.e. at $r = 10''$, on azimutally averaged profiles. The presence of a central nearly point-like peak due to radiation from the star in the CFHT and VLT *V* images was taken into account and a small correction was done when estimating the plateau maximum intensity at $r = 10''$. No *V* plateau photometry could be achieved from the OHP data because of an excessively strong central peak. The *B* and *V* surface brightnesses of Table 2 are not very different to previous values given by MH99, and supersede them. In *V*, the plateau is found to be 0.24 mag brighter than that found by Crabtree et al. (1987).

Figure 1 displays a composite image of the envelope in the *U* band, made by summing all the long OHP and short VLT *U* exposures (the summed number of photons per arcsec^2 emitted by the nebula is comparable in OHP and VLT observations). Comparison with the *B* and *V* images displayed in MH99 shows that, in the *U* filter, the nebula may be slightly brighter on the South-west side, which is the direction towards the galactic equator. This might be due to the UV-bright OB stars concentrated in the galactic plane, but a deeper image is obviously necessary to confirm this asymmetry.

Figure 2 shows azimuthally averaged profiles of the nebula. Each point corresponds to the signal average over a 4″-wide annulus. No sky subtraction has been done here. The ordinates are CCD counts (ADU) and the scales have been adjusted so that both the plateau and the sky are located at about the same level (dashed line) for any instrument and filter. This scaling could not be done for OHP *V* because the plateau is not well detected, and this profile is displayed here only to show the nebula extension at faint levels. This figure shows that there is no noticeable difference in the nebula shape as a function of wavelength, given the experimental uncertainties. It is worth noticing that despite the very low net signals in the *U*-band, i.e. 1.5 ADU at VLT, 5 ADU at OHP, the *U* profiles are well recovered thanks to the averaging over a large number (thousands) of pixels located in the annuli. The profiles show that

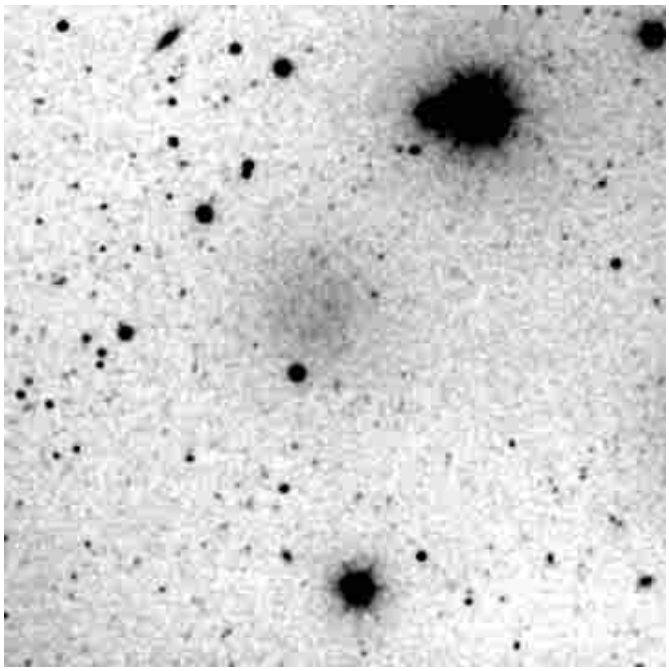

Fig. 1. Composite *U* image obtained by summing all *U* frames from OHP and VLT observations. The field is 6.0×6.0 arcmin^2, with 1.0″ pixel. North is up, East to the left.

the nebula is detected up to ~100 or ~200 arcsec, depending on instrument and bandwidth. These differences are instrumental effects. They reflect both various depths of the exposures and lack of background flatness at very faint levels.

The depth of the central depression is best measured in the *B* band. In this band the central core of IRC +10216 is a very faint point-like source, with $B \approx 25.2$ in the CFH frame. Its contribution can be easily subtracted, and the depression depth is found to be 17 ± 3 percent in *B*. Estimating the depth in *U* is much less accurate due to poor S/N in the central bin ($r < 4''$).

The half maximum radius of the profile is also best measured in *B* and is $R_{1/2} = 29'' \pm 2''$ from OHP and CFH data. There is no evidence for a larger $R_{1/2}$ value in *U*, taking into account experimental uncertainties (Fig. 2). Finally in the *V* band, $R_{1/2}$ is measurable with less accuracy, and is estimated to be around 27″.

4. Modelling

In order to interpret the observational data, we have to adopt quantitative characteristics for the ISRF and the circumstellar dust envelope (CSE), and the scattering of light by the dust has to be calculated. Our approach to the ISRF and the CSE parameters is to consider the most recent and plausible values derived from other studies (although as seen below, significant uncertainties exist), and to investigate whether they can explain the observations.

4.1. Parameters for the ISRF

We have considered two different sources for the ISRF. The first is that of Mathis et al. (1983, MMP83), who carried out a synthesis of various measurements and models in order to

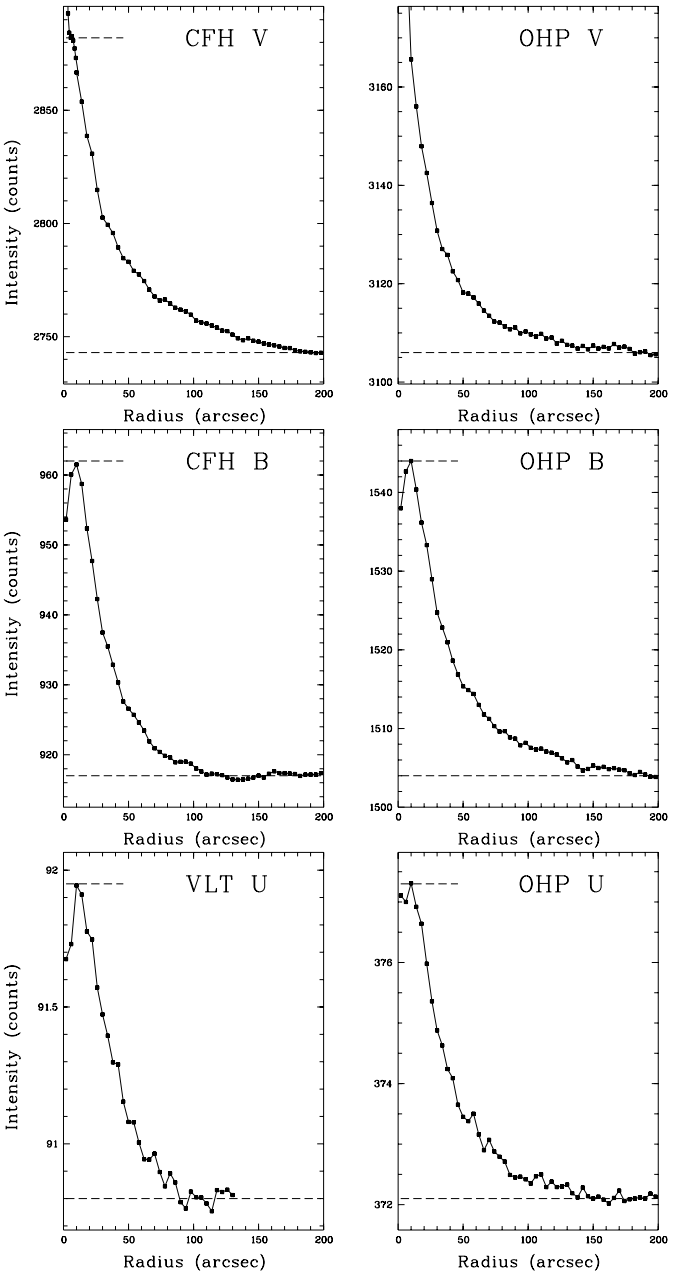

Fig. 2. Profiles of the IRC +10216 nebula in *UBV* bands. No sky subtraction has been done. The ordinate scales have been adjusted so that the background level and the nebula "plateau" (central zone within a radius of ∼15″) have in all panels the same levels, indicated by dashed horizontal lines.

derive ISRF values as a function of galactocentric distance, from far UV to far IR wavelengths. Table 3 reproduces the λ, $f(\lambda)$ values of their Table A3 for the solar neighbourhood (i.e. for $D_G = 10$ kpc as adopted by them). Corresponding apparent *UBV* magnitudes and colors were derived with the appropriate formulae of Allen (1973), which are indicated in the Table 3 notes.

The second work we considered is that of Mattila (1980a) who calculated synthetic spectra of the integrated stellar light (ISL) between 3000 Å and 10 000 Å in the solar neighbourhood. The diffuse galactic light, another component of the

Table 2. Results concerning the nebula of IRC +10216.

Quantity	Result
Plateau Surf. Bright. *U*	25.85 ± 0.15 mag arcsec^{-2}
Plateau Surf. Bright. *B*	25.70 ± 0.10 mag arcsec^{-2}
Plateau Surf. Bright. *V*	25.20 ± 0.10 mag arcsec^{-2}
Color $U - B$	0.15 ± 0.25
Color $B - V$	0.50 ± 0.20
Half-light radius in *B* & *U*	29 ± 2 arcsec
Central depression in *B*	17 ± 3 percent

ISRF in addition to direct starlight and which comes from light scattered by dust, is not modelled in that work. However, according to Mattila (1980b), its effect on the total radiation density averaged over the whole sky is estimated to be small, of the order of 20%. Here, we have chosen to ignore this small component for clarity. Table V of Mattila (1980a) provides *UBV* surface brightness estimates of the ISL, assumed here to be equal to the ISRF, in the solar neighbourhood and in units of S10, where one S10 is one 10th magnitude star per square degree. They were converted into apparent *UBV* magnitudes by integrating over the sky (41 253 sq deg). The corresponding fluxes $f(\lambda)$ derived with Allen's formulae are also given in Table 3.

Table 3 shows that these two ISRFs agree in *B* and *V* ISRF fluxes (and $B - V$ color), but a difference of 0.45 mag is found in the *U* band (i.e. a factor of 1.5), in the sense that the Mathis ISRF is bluer in $U - B$. Mattila (1980a,b) found in his synthetized ISL a large flux jump between 3500 Å and 4200 Å which results from the Balmer jump of A-type stars and the discontinuity at 4000 Å from late-type stars. In contrast, the MMP83 ISRF is expressed by 3 blackbodies *plus* an UV component for $\lambda < 2500$ Å, and this approximation is said to be within 15 percent (or better) of the various observational data over the full spectral range (see MMP83, and also Mezger et al. 1982, their Appendix C). Therefore, at this stage, we find it interesting to keep both approaches for further discussion.

4.2. Parameters for the dust envelope of IRC +10216

Concerning the CSE of IRC +10216, we have adopted as a baseline the results of Groenewegen (1997, herafter G97), who considered a large number of constraining observations (that probe mostly, but not exclusively, the inner layers of the CSE). The adopted parameters are listed in Table 4. Although the CSE is known to show multiple shells (MH99, Mauron & Huggins 2000), we assume a smooth and spherically symmetric density distribution and will attempt to reproduce azimuthally-averaged profiles, leaving the consequences of the non-radial envelope structure for future study. With an assumed distance of 135 pc, G97 estimates a dust mass-loss rate of $1.1 \times 10^{-7}\ M_\odot\ \mathrm{yr}^{-1}$ beyond 4.47 stellar radii (inner envelope radius). Furthermore, we considered an outer envelope radius of 210″ ($R_{\rm out} = 6000\ R_*$) corresponding to the most distant material detected by Mauron & Huggins (1999). This is certainly a lower limit for the IRC +10216 envelope outer radius since

Table 3. Characteristics of the ISRF.

λ (μm)	$f(\lambda)$ (erg cm^{-2} s^{-1} Å^{-1})	Magnitudes	Notes
	from Mathis et al. (1983)		
0.346	1.30 E−6	$U = -6.21$	(1)
0.435	1.50 E−6	$B = -5.89$	(1)
0.550	1.57 E−6	$V = -6.54$	(1)
		$U - B = -0.32$	
		$B - V = +0.65$	
	from Mattila (1980a)		
0.365	0.87 E−6	$U = -5.76$	(2)
0.440	1.47 E−6	$B = -5.87$	(2)
0.550	1.52 E−6	$V = -6.52$	(2)
		$U - B = +0.11$	
		$B - V = +0.65$	

Notes:
(1) *UBV* are derived with:
$U = -2.5\ \log_{10} f(0.365) - 20.925$,
$B = -2.5\ \log_{10} f(0.44) - 20.450$,
$V = -2.5\ \log_{10} f(0.55) - 21.050$.
(2) $f(\lambda)$ derived from *UBV* data with above formulae.

Table 4. Characteristics of the envelope of IRC +10216.

Parameter	Value	
Standard model (0.16-μm grains)		
Distance d	135 pc	
Central star $T_{\rm eff}$	2000 K	
Central star radius R_*	35 mas	
Dust density law	$\rho_{\rm d} \propto r^{-2}$	
Inner envelope radius $R_{\rm in}$	4.47 R_*	
Outer envelope radius $R_{\rm out}$	6000 R_*	
Dust mass loss $\dot{M}_{\rm d}$	$1.1\,10^{-7}\ M_\odot$ yr^{-1}	
Grain velocity $v_{\rm d}$	17.5 km s^{-1}	
Grain radius a	0.16 μm	
Grain density $\rho_{\rm d}$	2.0 g cm^{-3}	
Dust optical properties	amorphous carbon	(1)
Radial opacities τ_U, τ_B, τ_V	77.1, 84.3, 80.2	(2)
Small grain model (0.05-μm grains)		
Same parameters as above except:		
Grain radius a	0.05 μm	
Radial opacities τ_U, τ_B, τ_V	66.7, 41.3, 24.0	(2)

Notes:
(1) Type AC1 from Rouleau & Martin (1991).
(2) Radial opacities like τ_U are also noted $\tau_{U,\,\rm rad}$ in the text.

Young et al. (1993) found dust twice as far away using IRAS data. However, we checked that our results concerning the model brightnesses and colors of the IRC +10216 nebula are independent of $R_{\rm out}$. Considering a larger outer radius would only lead to a slightly larger width of the brightness profiles (see the discussion below).

As recommended by G97, the grains considered here are spherical particles with a single size ($a = 0.16\ \mu$m), and their composition is that of amorphous carbon with optical properties given by Rouleau & Martin (1991, labelled AC1 in their Table 1; see also Appendix C). This table also indicates another possible choice for the grain radius, $a = 0.05\ \mu$m (as found by MR87 and discussed below). It has to be noted that silicon carbide grains are also found in the envelope of IRC +10216. However, since (i) only a few percent of the dust grains are found in SiC form, and (ii) their opacity effects are mostly seen around 11 μm and are completely negligible in the optical, we do not consider such grains in our model.

With the parameters of Table 4 (standard model, with $a = 0.16\ \mu$m), the radial optical thickness of the envelope in B (taken from the inner to the outer radius of the envelope) $\tau_{B,\,\rm rad}$ is equal to 84.3, in excellent agreement with G97 if he neglected SiC grains. The observed spectral energy distribution of IRC +10216 is well reproduced by our model except for some small departures around 11 μm in the SiC signatures.

The optical thickness of the nebula *along the line of sight* at θ arcseconds from the center can be written as:

$$\tau_\lambda(\theta) = \pi\,\tau_{\lambda,\,\rm rad}\ \frac{\theta_{\rm in}}{\theta}\ q\left[\frac{2}{\pi}\ \arctan\left(\frac{\sqrt{1-u^2}}{u}\right)\right]. \qquad (1)$$

Here, $\tau_{\lambda,\,\rm rad}$ is the radial optical thickness of the envelope (i.e. from the center of the nebula up to $R_{\rm out}$); $\theta_{\rm in} = R_{\rm in}/d$ corresponds to the angular inner radius of the envelope; $\theta_{\rm out} = R_{\rm out}/d$. The factor q is very close to 1.0 and can be ignored: rigourously $q = 1/(1 - R_{\rm in}/R_{\rm out})$. The quantity u is $\theta/\theta_{\rm out}$, and the factor $[\frac{2}{\pi}\ \arctan()]$ is the effect of the outer envelope limit, and is equal to 1 if no outer limit is assumed.

With the parameters of Table 4, and for an angular distance from the center of 50″, the standard model predicts in the B filter a line of sight opacity $\tau_B(50'') = 0.70$. The factor in brackets due to the external edge is 0.85 and an unlimited envelope with the same $\tau_{\lambda,\,\rm rad}$ would have an opacity 15 percent larger, i.e. 0.82. At 100″, one finds $\tau_B(100'') = 0.28$. Therefore, the model envelope is optically thick in the observed region for offsets between 0 and ~100–200″, and a radiative transfer code is needed to predict the nebula optical surface brightness.

4.3. The Monte-Carlo radiative transfer code

In order to model ISRF illumination, we have developed a specific radiative transfer code based on an upgraded version of the one described in Lopez et al. (1995). Although the code has been built to allow for non-spherical dust density distributions, we consider in the present work spherically symmetric envelopes with a radial power-law distribution of the form $N(r) = N_{\rm in} \times (R_{\rm in}/r)^{-n}$, where r is the radial distance from the star with $R_{\rm in} < r < R_{\rm out}$, and $N(r)$ is the number density of grains. The dust grains are assumed to be homogeneous and spherical with a single radius a. Their optical properties, i.e. the extinction $Q_{\rm ext}$, scattering $Q_{\rm scat}$, and absorption $Q_{\rm abs}$ efficiencies, and the scattering phase function, are derived from optical indices using Mie theory. Finally, the optical thickness of the envelope at the wavelength λ is defined by

$$\tau_{\lambda,\,\rm rad} = \int_{R_{\rm in}}^{R_{\rm out}} N(r)\pi a^2\, Q_{\rm ext}(\lambda)\,{\rm d}r. \qquad (2)$$

Two sources of illuminating radiation can be considered in the code: the first is the central star with radius $R_\star$ and assumed to radiate as a blackbody of a given effective temperature. This source is considered only for computing the spectral energy distribution (SED), found to be in full agreement with that of G97. The transfer of radiation in the dust and the radiative equilibrium of the grains are numerically solved by a Monte-Carlo method at 30 different wavelengths, and more details are given in Lopez et al. (1995).

The second source is the ISRF, whose spectral energy distribution is taken either from MMP83 or from Mattila (1980a). The ISRF is synthesized using a large light-emitting sphere centered on the nebula. The surface brightness of the sphere varies as cosϕ, where ϕ is the inclination angle to its normal, and is equal for $\phi = 0$ to $f(\lambda)/4\pi$ (in erg cm^2 s^{-1} Å^{-1} sr^{-1}), where $f(\lambda)$ is the ISRF value as given in Table 3. The radius of this ISRF sphere is larger than the outer radius of the envelope, and it can be shown that each point inside this ISRF sphere receives in the absence of matter a homogeneous and isotropic photon flux equal to the ISRF.

In order to obtain a model image to compare with the *UBV* observations described above, we consider only ISRF photons emitted by the sphere that have been actually scattered by dust grains in the envelope, and we ignore those directly emitted towards the observer and passing through the envelope without any interaction. This has to be done in order to avoid a bright background, which is not observed. The reason is that in the reality (but not in our model), the ISRF photons come mainly from individual point-like sources (the stars). The contribution of diffuse light scattered by the galactic cirrus and interstellar clouds is small, and this is especially true for ISRF photons coming from behind IRC +10216, which is at $l = 221°$, $b = +45°$. Within ∼2° of IRC +10216, little interstellar extinction is detected, since an estimate $E(B-V) \leq 0.03$ mag can be obtained from the maps of Burnstein & Heiles (1982) and those of Schlegel et al. (1998). For such a low extinction, the observations of Guhathakurta & Tyson (1989) suggest that the diffuse galactic background should be of the order of 27–28 *B*-mag arcsec^{-2}. This is more than 25 times less than the ISRF surface brightness when it is averaged over the sky (this spatial average is equal to 23.44 *B*-mag arcsec^{-2}). Consequently, in order to avoid in our model this fictitious, high background of 23.44 *B*-mag arcsec^{-2}, direct photons, which are emitted by the ISRF sphere but are eventually not scattered by the envelope, are ignored.

In the *UBV* range considered here, the model envelope brightness is entirely due to scattered ISRF photons since (i) its optical depth is so large that no photons from the star can escape and (ii) the radiation emitted by the heated dust is insignificant in visible light. Therefore, no central star was implemented in our simulation. For a given set of parameters and for each wavelength, the code returns an image of the externally illuminated envelope. Radial brightness profiles are then derived. To get a profile with a reasonably low noise, around 20 million events ("scattered photons") are considered per Monte-Carlo simulation and the computation time in parallel mode is about 5 hours on a Compaq AlphaServer equipped with four 525 MHz microprocessors.

5. Model results, interpretation and discussion

We consider here the results of modelling when *standard* envelope parameters are adopted (i.e. Table 4, with 0.16 μm grains), and compare them with the observations. We also discuss a model where the grain size is changed to 0.05 μm while keeping the same dust mass loss rate and other parameters. This 0.05-μm model reproduces the observed SED reasonably well (see Fig. 3 of G97), and its radial opacity τ_B is equal to 41.3, which is obtained by scaling the standard opacity with appropriate $Q_{\rm ext}$ and a values ($N(r) \propto a^{-3}$ and $\tau_B \propto Q_{\rm ext}/a$, see Eq. (2)).

5.1. Analysis of the central part of the nebula

The first issue concerns the intensity and shape of the nebula in its central part, within ∼50″ of the center. The *B* band is particularly suitable for consideration because there is no difference between Mathis's and Mattila's ISRFs in *B*, and because the plateau in *B* is free from a central bright source like in *V*. Figure 3 shows that the agreement is poor between the standard model and observations. In order to reproduce the *B*-band plateau maximum surface brightness, one has to divide the model intensity by a factor of 2.3: this factor is clearly too large to be attributed to photometric measurement errors on the plateau brightness. Secondly, concerning the shape itself, the model profile is found to be much broader that the observed one. While the model predicts a radius at half intensity, $R_{1/2}$ of 73″, the observation gives $R_{1/2} = 29'' \pm 2''$. One notes in Fig. 3 that there is some disagreement between the *B* profiles obtained at OHP and CFH, due to experimental difficulties described in Sect. 2, but this concerns large offsets and essentially does not affect the $R_{1/2}$ value of 29″. Figure 3 also shows the *B* profile for 0.05-μm grains: in this case, there is a nice agreement on the plateau level, but the model profile is still too broad, with $R_{1/2} = 54''$.

The second issue is the wavelength dependence of the nebula shape (shape chromatism). Figure 4 shows the model profiles in *UBV* for the two grain sizes. In each case, we have normalized the *UBV* profiles at the same (arbitrary) maximum value, so that only the shapes are considered. In the standard case (0.16 μm grains), the shape is the same for *U*, *B*, or *V* and the profiles are exactly superposed. In contrast, if 0.05 μm grains are adopted, there is a strong chromatism in the sense that the *U* profile is much broader than the *V* one. More precisely, for a 0.16 μm grain, $R_{1/2} = 73''$ for all filters, whereas for 0.05 μm, one has $R_{1/2} = 71''$, 54″, 29″ for *U*, *B*, *V* respectively. This situation is entirely due to the fact that small grains scatter nearly in the Rayleigh regime, with strong color effects, while larger grains are grey. Because the observations show no chromatism (see Fig. 2) and negligible variation of $R_{1/2}$ with wavelength, the larger grain size (0.16 μm) is clearly favoured. It is however true that for small grains the *V*-band $R_{1/2}$ value fits the observation (29″) rather well, but there is a large and increasing discrepancy for *B* and *U* bands.

The third issue concerns the colors of the nebula. Figure 5 shows that the observed plateau colors are relatively close to those predicted for the Mattila's field scattered by 0.16 μm

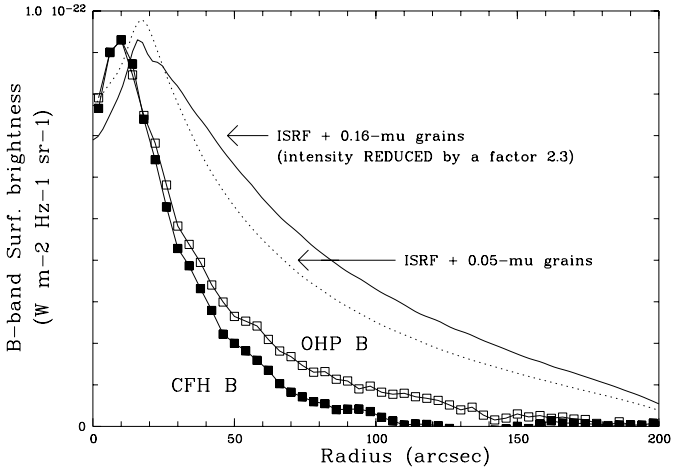

Fig. 3. Model brightness profile of IRC +10216 computed in *B* (0.435 μm) (thin continuous line). The envelope parameters are standard (Table 4, $a = 0.16$ μm). For clarity of the plot, the intensity of this profile is drawn after arbitrarily dividing it by a factor 2.3 in order to fit the plateau intensity. The data from OHP and CFH are also shown (dots), together with the actual model profile for $a = 0.05$ μm (dotted line).

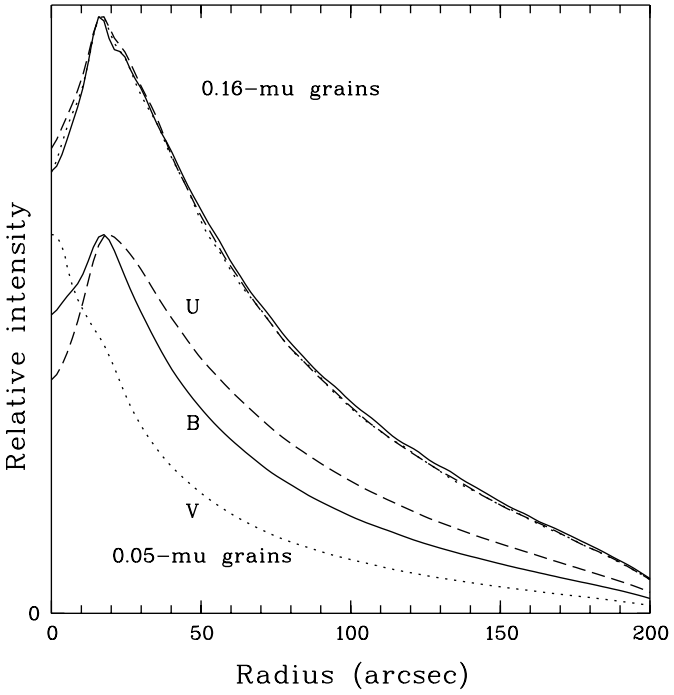

Fig. 4. Normalized model profiles for *UBV* bands and for grain sizes of 0.16 and 0.05 μm. The 0.16 μm profiles are found to be almost similar (shape achromatism). In contrast, the 0.05 μm profiles (shifted down by an arbitrary factor for clarity) clearly depend on wavelength.

grains. Actually, the agreement is better between the observed colors and the colors of Mattila's field itself, suggesting pure grey scattering by circumstellar grains, i.e. large sizes. One can also see that if 0.05 μm grains are adopted, none of the fields match the observed colors. Adopting the field of Mathis and 0.16 μm grains is worse than adopting the field of Mattila and the same grains, especially when considering the $U - B$ index for which the two fields differ. We also note that when one compares the colors of the fields with those of the main sequence stars, the Mathis field seems surprisingly blue in $U - B$, as blue as an unreddened B8 star. If this was true, the rare stars bluer than B8 would have to compensate the many dwarf or giant stars redder than B8. It is much easier to understand the colors of Mattila's field, which is located at an average position in $U - B$ and $B - V$.

Given the above considerations, it does not appear possible with our data to settle the question of the dominant grain size. Both sizes (0.05 and 0.16 μm) present advantages and disavantages. The small size fits reasonably well the plateau intensity and shape *in the V band*, but fails for *B* and *U* (shape chromatism) and for the plateau colors. Regarding the large grain size (0.16 μm), the model intensity in *B* is too strong by a factor of 2.3 on the plateau, and also too strong by a factor as large as ∼10 for $\theta = 70''$ (Fig. 3). It is interesting to note that one cannot improve this situation by simply reducing the total opacity (or equivalently the dust mass loss rate) because this produces an even stronger peak at center and disappearance of the central depression, as shown in Fig. 6. We have also explored grains larger than 0.16 μm: with AC1 material, a satisfactory value of $R_{1/2}$ is obtained for $a = 0.28$ μm (then, in the *B* band, $\tau_{B,\,\mathrm{rad}} = 34.4$) but the profile does not show any central depression, and the plateau level is still two times too high compared to observation.

A better fit to the profile is obtained by reducing progressively the dust mass loss rate of the standard model in the outer regions. For example, a density decrease in r^{-4} at $r > 20''$ produces a satisfactory $R_{1/2} = 29''$ (a r^{-3} law is not enough), although the plateau remains too high.

5.2. Analysis of outer regions ($\theta \geq 70''$)

There is another way of analysing the data: instead of considering the main part of the nebula and the plateau characteristics, one can focus on the outer layers, say at $\theta = 70''$. At this radial distance, the surface brightness is certainly less accurately measured than at its center, but its faintness suggests that the envelope can be considered as optically thin at this distance, which greatly simplifies the modelling. Optical thinness is also supported by the fact that the density of background galaxies in a recent very deep *V*-band VLT image (de Laverny 2002) is found to be very similar at $\theta \sim 70''$ and farther out. Then, a grain located at this radius is illuminated by almost a pure ISRF for several reasons: i) the grain sees the central region of the nebula over ∼50 degrees *FWHM*, i.e. over a small solid angle of ∼0.6 sr, which is much less than 4π sr, and ii) the average surface brightness of the nebula as seen by the grain is fainter than 25.7 mag/arcsec^2, which is small against the average ISRF brightness of 23.44 mag/arcsec^2 in the *B*-band; iii) most of the directions seen by the grain are optically thin. Consequently, in the optically thin regime and with an isotropic illumination, the

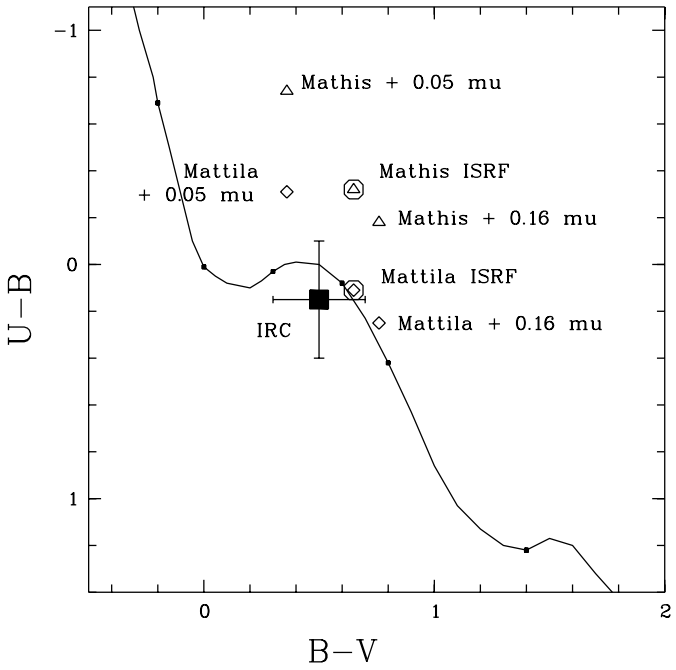

Fig. 5. Comparison of the plateau *UBV* colors with models. The solid black dot with error bars and labelled IRC represents the observed colors of the plateau. The labelled triangles and lozenges represent the model plateau colors. Concerning the fields, the ISRF of Mathis et al. is represented by an encircled triangle, and that of Mattila by an encircled lozenge. The line shows the *UBV* locus of main sequence stars, with dots indicating the positions of B3, A0, F0, G0, K0, and M0-type stars.

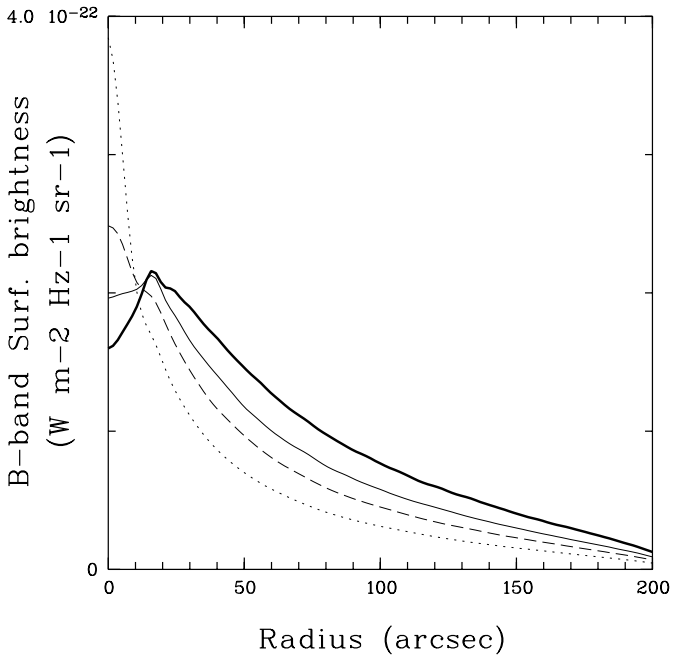

Fig. 6. Evolution of the model profile in B light when $\tau_{B,\,\mathrm{rad}}$ is decreased from $\tau_{B,\,\mathrm{rad}} = 84$ (standard model, 0.16 μm grains, thick solid line), to $\tau_{B,\,\mathrm{rad}} = 80$ (thin solid line), $\tau_{B,\,\mathrm{rad}} = 60$ (dashed) and $\tau_{B,\,\mathrm{rad}} = 45$ (dotted). Note that the *observed* plateau maximum brightness is at 0.92×10^{-22} W m^{-2} Hz^{-1} sr^{-1}.

surface brightness of the dust envelope at a large angle θ can be written (see, e.g., Guhathakurta & Tyson 1989):

$$S_\lambda(\theta) = \frac{1}{4\pi}\, f_\lambda\ \omega\ \tau_\lambda(\theta), \tag{3}$$

where $S_\lambda(\theta)$ has the units of ISRF flux f_λ per steradian, ω is the grain albedo, and $\tau_\lambda(\theta)$ is the line of sight optical opacity at offset θ. For an unlimited r^{-2} envelope, this opacity can be expressed as:

$$\tau_\lambda(\theta) = \frac{3}{16}\ \frac{Q_\mathrm{e}}{a\rho_\mathrm{d}}\ \frac{\dot{M}_\mathrm{d}}{v_\mathrm{d}\, d}\ \frac{1}{\theta}, \tag{4}$$

and finally:

$$S_\lambda(\theta) = \frac{3}{64\pi}\ f_\lambda\ \frac{Q_\mathrm{sca}}{a}\ \frac{\dot{M}_\mathrm{d}}{v_\mathrm{d}\rho_\mathrm{d} d}\ \frac{1}{\theta}. \tag{5}$$

In principle, the θ^{-1} dependance of Eq. (5) might be checked on the observed profiles, but in practice, this is hardly possible because of the faintness of the signal and its uncertainties at these large offsets (see Sect. 2, and Figs. 2 and 3).

In Eq. (5), we can reasonably consider that the grain velocity v_d, the grain density ρ_d, the distance d and the ISRF strength f_λ are relatively well known (Tables 3 and 4). Then, because the B-band observations provide at $\theta = 70''$ a surface brightness $S_B(\theta)$ of $\sim 4.4 \times 10^{-20}$ erg cm^{-2} s^{-1} Å^{-1} arcsec^{-2} (with an uncertainty of about a factor 2), one gets the following constraint:

$$\frac{\dot{M}_\mathrm{d}}{1.1 \times 10^{-7}\ M_\odot\ \mathrm{yr}^{-1}} \times \frac{Q_\mathrm{sca}}{a_\mu} \approx 0.60. \tag{6}$$

For $a = 0.16\ \mu$m and $\dot{M}_\mathrm{d} = 1.1 \times 10^{-7}\ \ M_\odot\ \mathrm{yr}^{-1}$, which is the "standard case", $Q_\mathrm{sca} = 2.16$ and $Q_\mathrm{sca}/a_\mu = 13.5$. This means that the model flux is found to be ~22 times larger than observed. However, in this case, the line of sight opacity $\tau_B(70'')$ is 0.58, so that the optically thin approximation is invalid here. Figure 3 illustrates this case more rigourously and indicates a factor of ≈9 for the excess of model flux at 70″.

In order to improve the agreement between model and observations, a lower $\dot{M}_\mathrm{d}$ or a lower value for Q_sca/a_μ are needed, or both, i.e., less dust or dust with a poorer scattering efficiency. If $a = 0.05\ \mu$m, $Q_\mathrm{sca}/a_\mu = 4.1$ and Eq. (6) implies that $\dot{M}_\mathrm{d}$ should be as low as $0.16 \times 10^{-7}\ M_\odot\,\mathrm{yr}^{-1}$, and then $\tau_B(70'') = 0.042$. This "small grain – small dust loss" solution can reproduce the faintness of the nebula at large offsets, but in no case can it account for the central region when extrapolated down to inner layers, because the radial opacity of the whole envelope would be $\tau_{B,\,\mathrm{rad}} \approx 6$ ($\tau_{B,\,\mathrm{rad}}$ is equal to $\frac{1}{\pi}\ \tau_B(\theta)\ \theta/\theta_\mathrm{inn}$), largely insufficient to produce a plateau. This solution cannot account also for the observed polarized intensity in the near infrared reported by Tamura et al. (1988).

Larger grains can also be envisaged, and for example with $a = 0.28\ \mu$m, Q_sca/a_μ is also equal to 4.1; then from Eq. (6), one finds again $\dot{M}_\mathrm{d} \sim 0.16 \times 10^{-7}$. In this case, $\tau_B(70'') = 0.035$ and the envelope radial opacity is found to be $\tau_{B,\,\mathrm{rad}} \approx 5$, again largely insufficient to make a central plateau.

5.3. Discussion

The above analysis illustrates the fact that it is not easy to reproduce with simple models all the envelope observations. The standard model, which is based on the results of G97 and fits

a lot of observations of dust in IRC +10216, especially in the infrared, fails to account for several features of the nebula seen in scattered galactic light. In particular, it seems difficult to simultaneously reproduce the plateau level, its profile, and the faintness of the outer regions.

These difficulties may be due, at least in part, to our simplified treatment of dust. Grain scattering depends primarily on dust optical properties (indices) and the grain size. Scattering also depends on factors like particle porosity and asphericity, and consequently the applicability of the Mie theory. How large the effects of these last two factors are is difficult to estimate without extensive calculations that are beyond the scope of this work. We have also refrained from trying to search for a better agreement between model and observations by simply tuning the optical properties, i.e., modifying at each wavelength the optical indices. The reasons are that G97 used the Rouleau & Martin AC1-type amorphous carbon indices, and, for consistency, the same optical properties should be used here as far as possible; secondly, the indices must obey the Kramers-Kronig relations and cannot be arbitrarily modified in a limited wavelength domain. In summary, our approach has been to consider only two different single particle sizes (0.16 and 0.05 μm), and these two cases correspond to very different albedos and anisotropy g factors: compared to the standard case (0.16 μm grains), the 0.05 μm grains have a lower albedo, which gives a very satisfactory fitting of the plateau intensity, but these small grains produce too much chromatism because their albedo strongly depends on wavelength (see above and Appendix C for more details on adopted indices, albedos, etc.). It would certainly be interesting to envisage in future work a grain size distribution, although, to our knowledge, no robust observational constraint on circumstellar grain size distributions is presently available (see also the arguments given by G97 for considering only a single grain size).

Our analysis suggests that reducing the dust loss rate at large offsets (>25 arcsec, corresponding to 1000 yrs ago) is a possible solution to explain the nebula shape and its radial width. Variability of mass-loss with various time scales is a well-known characteristic of AGB stars (see for example the references in Olofsson 1999 or in Marengo et al. 2001), and mass-loss variations for evolved carbon stars is also theoretically predicted (e.g. Wachter et al. 2002). Concerning IRC +10216 itself, observations of its extended envelope in the CO millimeter emission lines have been studied by Huggins et al. (1988), and more recently by Groenewegen et al. (1998). The last authors conclude, from their analysis of the CO line profiles and maps, that the mass loss is enhanced by a factor of ~5 for $\theta > 50''$ compared to inner layers. Such a density enhancement is clearly not seen in our radial profiles, and we checked that if one modifies the standard model by increasing $\dot{M}_{\rm d}$ by ~5 for $\theta > 50''$, a huge bump appears in the envelope profile, and such a bump is definitively not observed (Figs. 2 and 3). Thus, our data tend to suggest that the CO "excess" emission at large offsets is either due, perhaps, to incompletely corrected instrumental lobe effects, or, if real, that they are the consequences of a physical phenomenon different from a density enhancement, as originally proposed by Huggins et al. (1988).

Concerning the faintness of the nebula, especially at large offsets, it is also interesting to compare the present case of IRC +10216 with the optical studies of high latitude clouds (Guhatakurta & Tyson 1989). These clouds, that absorb and reflect the ISRF, are found to be, in the visible range, about 10 times fainter than predicted by models which reproduce their infrared radiation (with an *isotropic* ISRF). The optical faintness of these clouds and that of the outer layers of IRC +10216 might be related. Perhaps, if the ISRF is not completely isotropic, both phenomena are due to grain forward scattering of the photons coming preferentially from the galactic plane and escaping away from the observer's view.

As for the interstellar radiation field, it seems presently premature to draw conclusions about its absolute strength (e.g. in the B band) with some accuracy, i.e. an accuracy better than a factor of 2, as was hoped originally when this work started. MR87 proposed that, as a possibility, the field might be a factor ~2.5 smaller than standard, but our calculations with essentially the same envelope characteristics and the same grain radius (0.05 μm) do not confirm this point (Fig. 3). We found no satisfactory reason to explain this inconsistency of results (see Appendix B for more details), but we do find that a fainter field improves the fit with 0.16 μm or larger grains of AC1-type. Concerning the field colors, our work suggests that the $U - B$ value of +0.11 found by Mattila (1980a) is probably more correct than the one (−0.32) from Mathis et al. (1983).

Clearly, improving the simple model presented here appears desirable in order to reach (hopefully) firmer conclusions. One needs especially to estimate the effects of a grain size distribution, and if possible of grain porosity and asphericity. The effect of a field anisotropy should be investigated. In addition, the influence of envelope homogeneities and structure in discrete shells will have also to be considered, since it is known that clumpiness can significantly modify radiative transfer in envelopes (e.g. Mathis et al. 2002). In parallel with more sophistication in modelling, it would be fruitful to measure the colors of the nebula with less uncertainty, and extend the observations to red wavelengths (when the central variable star is at a minimum) and space ultraviolet. Imaging other similar nebulae might also bring valuable information on the properties of amorphous carbon dust and on the ISRF in the Galaxy.

6. Conclusions

We have presented new observations of the IRC +10216 nebula seen in the ambient galactic light, including the first U imaging. Additional images in B and V were obtained as well. These data were used to establish a UBV photometric sequence of nearby field stars, and to derive surface brightness profiles of the nebula, and UBV colors of the plateau. In blue light, where it is best observed, the nebula has a central depression of 17%, peaks at $\theta = 10''$, and its radius at half maximum $R_{1/2}$ is $29''$. There is no sign of an increased mass loss at ~$50''$, as CO maps may indicate.

The fact that the nebula shape, e.g. its half maximum intensity radius $R_{1/2}$, does not depend on wavelength suggests that grains scatter the galactic light in the grey regime. This conclusion is supported by the plateau colors which are close to

those of the ISRF as given by Mattila (1980a). The grain size of 0.16 μm recommended by Groenewegen (1997) is consistent with these aspects of the data; a smaller grain size like 0.05 μm would produce too strong a dependence of $R_{1/2}$ on wavelength and too blue a color. However, there remain important discrepancies between the 0.16 μm grain model and the observations, essentially concerning the intensity of the plateau and the $R_{1/2}$ value, which are better reproduced with 0.05 μm grains.

At first sight, our analysis suggests that the mass loss may be lower in the outer nebula, but reaching firm conclusions is difficult before assessing the effects of a grain size distribution, the envelope structure and perhaps some ISRF anisotropy. Given these uncertainties on grain properties and transfer modelling, there is also no firm evidence that the ISRF incident on IRC +10216 in the visible range is different from that usually taken in the solar neighbourhood.

Appendix A: *UBV* photometry of field stars near IRC +10216

In Table A.1, *UBV* photometry is given for 17 objects close to IRC +10216, derived from OHP observations. Coordinates (J2000) are from the APM catalog (Irwin and colleagues; `www.ast.cam.ac.uk/apmcat`). Objects with flag 1, in the last column, were used, when unsaturated, to calibrate the surface brightnesses of the IRC +10216 nebula in images from OHP, CFH and VLT. Objects with flag 2 are much redder than those with flag 1 ($B-V > 1.2$), and also redder than the nebula; consequently, they were not used for calibration. They are included here for completeness, as is Object 12 with flag 3 which is an elliptical galaxy.

Concerning the photometry, we do not pretend that its quality is the usual one for standard photometric sequences (i.e. ~0.01 mag), and our initial goal was more modestly to reach a ~0.1 mag uncertainty on colors. The *UBV* data result from aperture photometry made on only 2 to 5 images per color obtained during 3 nights (see the log in Table 1). Calibration on standard fields was limited in accuracy by the weather, which was not quite photometric, except during the night of deep *U* 1-hour exposures. The magnitudes and colors listed in Table A.1 were obtained by adopting plausible absorption coefficients for OHP, by including a color term in the transformation from instrumental to standard bandpasses, and by averaging the results from different exposures. The listed uncertainty is the *internal* error for colors, while it is 0.01–0.02 mag for *V*.

A first independent verification of the OHP photometry in *V* and *U* was achieved with the ESO VLT observations. The *V* and $U-V$ values from VLT were found to be within 0.04 and 0.03 mag of the OHP ones. A second verification was done by considering the color-color diagram of our photometry (Fig. A.1). This diagram shows a group of 10 stars with $B-V$ between 0.45 and 0.8 and located slightly (~0.15 mag) above the location of the Population I main sequence (continuous line). This situation is fully consistent with expectations for high latitude (IRC +10216 is at $b = +44°$), faint ($V = 14$ to 19) stars which statistically probe the metal-weak thick disk.

For instance, Ojha et al. (1999) provide $U-B$ vs. $B-V$ diagrams and $B-V$ histograms for two fields at $b = +47°$, and another exemple of $U-B$ vs. $B-V$ diagram for $b = +59°$ is given by Yamagata & Yoshii (1992). The $B-V$ edge of the stellar locus from these works is at about 0.4–0.45, exactly as in our data, and the $U-B$ average location is also in fair agreement with our work. Therefore, the final uncertainties of this approximate "sequence" should be probably of ±0.05 mag for *V*, and ±0.05 to 0.1 mag for $B-V$ and $U-B$ respectively, at least for (not red) objects flagged 1 used for calibrating the IRC +10216 surface brightness. The sequence is not the main source of error in the nebula surface brightness photometry, whose accuracy (0.1 mag in *V*, 0.2–0.25 mag in color indices) is more limited by its intrinsic faintness and sky level subtraction.

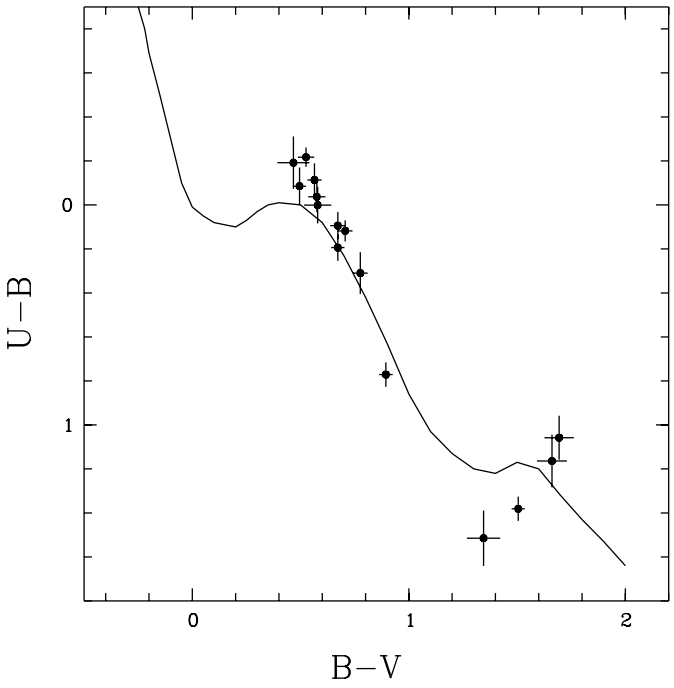

Fig. A.1. Color-color diagram for the field stars; the thin line is the Population I main sequence locus. Stars used for calibrating the nebula photometry have $B-V < 1$.

Appendix B: Quantitative verifications of the numerical code

Some numerical tests have been done in order to verify the consistency of the results returned by the code. They are in complete agreement with other computations or analytical relations.

First, the computed SED of IRC +10216 with the parameters of Table 4 is in excellent agreement with that published by G97. This increases confidence in the resolution of the radiative equilibrium equations.

Secondly, in order to check the computation of azimuthally-averaged brightness profiles (i.e. simulations of the ISRF illumination and scattering in the envelope), we considered the ideal case of an *optically thin* homogeneous sphere illuminated by an isotropic ISRF. We assume that the dust density is constant in the sphere of external angular radius $\theta_{\rm out}$. Because of optical thinness, each grain is illuminated by the ISRF itself,

Table A.1. *UBV* photometry of field stars near IRC +10216.

Num	α(2000)	δ(2000)	V	$B-V$	$U-B$	δ_{B-V}	δ_{U-B}	flag
1	09 47 59.84	+13 21 17.7	17.48	+0.67	+0.19	0.03	0.06	1
2	09 48 00.61	+13 20 08.6	16.87	+0.89	+0.77	0.03	0.06	1
3	09 47 58.66	+13 18 56.4	15.83	+0.71	+0.12	0.03	0.05	1
4	09 48 01.46	+13 17 37.0	16.23	+0.56	−0.11	0.03	0.08	1
5	09 48 04.35	+13 16 32.2	17.27	+0.52	−0.22	0.04	0.04	1
6	09 47 57.98	+13 16 09.9	16.00	+0.78	+0.31	0.03	0.09	1
7	09 47 49.47	+13 19 41.0	16.49	+0.57	−0.04	0.04	0.07	1
8	09 47 44.80	+13 19 15.0	14.33	+0.58	+0.00	0.06	0.08	1
9	09 47 42.76	+13 19 20.6	16.55	+0.67	+0.09	0.04	0.06	1
10	09 47 58.77	+13 15 07.7	17.53	+1.69	+1.06	0.07	0.10	2
11	09 48 06.79	+13 19 17.6	18.75	+0.50	−0.09	0.03	0.09	1
12	09 48 02.86	+13 19 11.5	18.44	+1.53	+0.25	0.05	0.08	3
13	09 48 00.41	+13 19 05.8	16.38	+1.50	+1.38	0.03	0.05	2
14	09 47 53.31	+13 14 31.3	19.32	+0.47	−0.19	0.07	0.12	1
15	09 47 46.05	+13 17 12.0	17.00	+1.35	+1.51	0.08	0.13	2
16	09 48 10.73	+13 18 12.0	17.50	+1.66	+1.16	0.07	0.12	2

and it can easily be shown that the surface brightness of such a sphere at an angle θ from its center can be expressed as:

$$S_\lambda(\theta) = \frac{1}{2\pi}\, f(\lambda)\, \frac{Q_{\rm sca}(\lambda)}{Q_{\rm ext}(\lambda)}\, \tau_{\lambda,\ {\rm rad}}\, \sqrt{1-\left(\frac{\theta}{\theta_{\rm out}}\right)^2} \qquad \text{(B.1)}$$

where $Q_{\rm sca}(\lambda)$ and $Q_{\rm ext}(\lambda)$ are respectively the scattering and extinction efficiencies at wavelength λ, $f(\lambda)$ the ISRF flux and $\tau_{\lambda,\ {\rm rad}}$ the radial optical thickness of the sphere (i.e. from center to outer radius). The brightness $S_\lambda(\theta)$ has the units of $f(\lambda)$ per steradian. An agreement better than 1% is obtained between the numerical and analytic brightness profiles for $\tau_{\lambda,\ {\rm rad}} \leq 0.01$, i.e. when the single scattering assumption remains correct. This test validates our treatement of ISRF illumination with an external sphere.

Thirdly, for an optically thin circumstellar envelope with a radial density varying as r^{-2}, the brightness profile can also be analytically estimated (for $\theta \geq \theta_{\rm inn}$):

$$S_\lambda(\theta) \;=\; \frac{1}{4}\, f(\lambda)\, \frac{Q_{\rm sca}(\lambda)}{Q_{\rm ext}(\lambda)}\, \tau_{\lambda,\ {\rm rad}}\, \frac{\theta_{\rm inn}}{\theta}\, q' \qquad \text{(B.2)}$$

where $q' = 1$ if no outer limit is assumed:

$$q' = \left(1-\frac{R_{\rm inn}}{R_{\rm out}}\right)^{-1}\, \frac{2}{\pi}\, \arctan\left(\frac{\sqrt{1-u^2}}{u}\right) \qquad \text{(B.3)}$$

with $R_{\rm inn}$ and $R_{\rm out}$ being the inner and outer envelope radius respectively, $\theta_{\rm out} = R_{\rm out}/d$ and $u = \theta/\theta_{\rm out}$. In this case also, the code returns very good results in comparison to this analytical brightness profile, provided that $\tau_{\lambda,\ {\rm rad}}$ is low enough.

We have also examined the case of similar but optically thicker spheres. For homogeneous spheres, our simulations show that the brightness profiles depart from the above Eq. (C.1) when multiple scattering plays a role, i.e. around $\tau_{\lambda,\ {\rm rad}} > 0.1$. An almost constant brightness profile with θ is obtained for $\tau_{\lambda,\ {\rm rad}} \sim 1$ and bright-rimmed spheres with dark cores are found for optically thicker cases. We also found that for optically thick spheres with radial density varying as r^{-2}, the surface brightness shows a minimum at the center, reaches a maximum at some angular distance from the center and then decreases strongly. All these results are entirely consistent with previous similar simulations such as those found in Witt & Stephens (1974, see their Figs. 1 and 2).

Finally, we have attempted to exactly reproduce the numerical results of Martin & Rogers (1987). One can first note that their Fig. 8 shows a significant chromatism of the plateau profile between the I and the V bands (0.81 μ and 0.55 μ) that is qualitatively consistent with our findings explained in Sect. 5. At 0.55 μm, *for a standard ISRF*, their modelled plateau is at 2.7 fu (flux unit, where 1 fu is 10^{-22} W m^{-2} Hz^{-1} sr^{-1}), extends to $\theta \sim 5''$, and has $R_{1/2} \sim 25''$.

Their model has essentially the same physical and geometrical properties as ours, but unfortunately their optical grain properties are not given in an explicit way. It is mentioned in their Sect. III-i that in V, $\omega = 0.38$ and $g = 0.10$. In addition, from their Fig. 1 where $Q_{\rm abs}/a$ and $Q_{\rm sca}/a$ are plotted, one can estimate $Q_{\rm abs} \sim 0.21$ and $Q_{\rm sca} \sim 0.15$. Using the Mie theory, with $a = 0.05$ μm and $\lambda = 0.55$ μm, one finds corresponding indices $n = 2.470$ $k = 0.264$, for which $\omega = 0.384$ and $g = 0.15$, $Q_{\rm a} = 0.221$, $Q_{\rm s} = 0.138$, $Q_{\rm e} = 0.359$, so that only g is discrepant (we have found no reason for that discrepancy). The model of Martin & Rogers has also $\tau_{11\mu} = 0.8$ and from their Fig. 1, $Q_{\rm e}(11\ \mu) = Q_{\rm a} = 0.0125$. Therefore, $\tau_{0.55\mu} = \tau_{11\mu} \times Q_{\rm e}(V)/Q_{\rm e}(11\ \mu) = 23.0$, in fair agreement with the value of 21 mentioned by them.

With $\tau_{0.55\mu} = 23$ and the n, k values found above, our code finds for a standard ISRF a very peaked central maximum at 2.75 fu, *with no plateau* and $R_{1/2} \sim 15''$. Only when $\tau_{0.55\mu}$ is increased to 30 does one get a plateau with maximum intensity of 2.0 fu, extended over $5''$ and with $R_{1/2} \sim 36''$. These two cases bracket the result of MR87, but are significantly

Table C.1. Grain optical properties.

				$a = 0.16\ \mu$m			$a = 0.05\ \mu$m		
Material	λ (μm)	n	k	Q_e	ω	g	Q_e	ω	g
AC1	0.365 (U)	1.970	0.236	3.297	0.53	0.85	0.892	0.46	0.27
AC1	0.435 (B)	1.966	0.233	3.604	0.60	0.81	0.556	0.37	0.18
AC1	0.550 (V)	1.981	0.232	3.429	0.63	0.75	0.321	0.25	0.11

different. Therefore, there are some differences between the results of Martin & Rogers and those obtained with our code, but it is difficult to say whether they are due to differences in the codes themselves or due to differences in indices.

Appendix C: Grain optical properties

Table C.1 lists the optical properties adopted in this work (amorphous carbon of type AC1 from Rouleau & Martin 1991).

Acknowledgements. The authors thank the anonymous referee and P. J. Huggins for comments that helped us improve the paper. We also thank B. Gladman for careful reading of the manuscript. Part of this work has been performed using the computing facilities provided by the program "Simulations Interactives et Visualisation en Astronomie et Mécanique (SIVAM)" at Observatoire de la Côte d'Azur. We acknowledge support from the CNRS Program *Physico-chimie du milieu interstellaire* (to N.M.), the CNRS-INSU *Actions thématiques innovantes* and the Ministère de l'Éducation Nationale et de la Recherche (to P.d.L.).

References

Allen, C. W. 1973, Astrophysical Quantities, 3rd edn. (London: The Athlone Press)
Arp, H. C., & Johnson, H. L. 1955, ApJ, 122, 171
Burstein, D., & Heiles, C. 1982, AJ, 87, 1165
Crabtree, D. R., McLaren, R. A., & Christian, C. A. 1987, in Late Stages of Stellar Evolution, ed. S. Kwok, & S. P. Pottasch (Dordrecht: Reidel), 145
Crabtree, D. R., & Rogers, C. 1992, Circumstellar Envelopes Observed as Optical Haloes, in Mass Loss on the AGB and beyond, ed. H. E. Schwarz, ESO Conf. & Workshop Proceedings, 46, 255
Glassgold, A. E. 1996, ARA&A, 34, 241
Groenewegen, M. A. C. 1997, A&A, 317, 503 (G97)
Groenewegen, M. A. C., Van de Veen, W. E. C. J., & Matthews, H. E. 1998, AA, 338, 491
Guhathakurta, P., & Tyson, J. A. 1989, ApJ, 346, 773
Habing, H. J. 1968, BAN, 19, 421
Huggins, P. J., Olofsson, H., & Johansson, L. E. B. 1988, ApJ, 332, 1009
Ilovaisky, S. 1997, Web site of the Haute Provence Observatory, Description of the 1.20 m telescope and its CCD camera `http://www.obs-hp.fr/`
Ivezic, Z., & Elitzur, M. 1996, MNRAS, 279, 1019
Jura, M. 1974, ApJ, 191, 375
Lagache, G., Abergel, A., Boulanger, F., et al. 1998, A&A, 333, 709,
de Laverny, P. 2002, in Mass-losing Pulsating Stars and their Circumstellar Matter, ed. Y. Nakada, & H. Honma (Dordrecht: Kluwer Academic Press)
Lopez, B., Mekarnia, D., & Lefèvre, J. 1995, A&A, 296, 752
Marengo, M., Ivezic, Z., & Knapp, G. R. 2001, MNRAS, 324, 117
Martin, P. G., & Rogers, C. 1987, ApJ, 322, 374 (MR87)
Mathis, J. S., Mezger, P. G., & Panagia, N. 1983, ADordrechtA, 128, 212 (MMP83)
Mathis, J. S., Whitney, B. A., & Wood, K. 2002, ApJ, 574, 812
Mattila, K. 1980a, A&AS, 39, 53
Mattila, K. 1980b, A&A, 82, 373
Mauron, N., & Huggins, P. J. 1999, A&A, 349, 203 (MH99)
Mauron, N., & Huggins, P. J. 2000, A&A, 359, 707
Mezger, P. G., Mathis, J. S., & Panagia, N. 1982, A&A, 105, 372
Ojha, D. K., Bienaimé, O., Mohan, V., & Robin, A. C. 1999, A&A, 351, 945
Olofsson, H. 1999, in Asymptotic Giant Branch Stars, ed. T. Le Bertre, A. Lèbre, & C. Waelkens, IAU Symp., 191, 3
Rouleau, F., & Martin, P. G. 1991, ApJ, 377, 526
Schlegel, D. J., Finkbeiner, D. P., & Davis, M. 1998, ApJ, 500, 525
Skinner, C. J., Meixner, M., & Bobrowsky, M. 1998, MNRAS, 300, L29
Tamura, M., Hasegawa, T., Ukita, N., et al. 1988, ApJ, 326, L17
van Dishoek, E. F. 1994, Photochemistry and The Interstellar Radiation Field, in The First Symposium on Infrared Cirrus and Diffuse Interstellar Clouds, ed. R. M. Cutri, & W. B. Latter, ASP Conf. Ser., 58, 319
Wachter, A., Schröder, K.-P., Winters, J. M., Arndt, T. U., & Sedlmayr, E. 2002, A&A, 384, 452
Witt, A. N., & Stephens, T. C. 1974, AJ, 79, 948
Yamagata, T., & Yoshii, Y. 1992, AJ, 103, 117
Young, K., Phillips, T. G., & Knapp, G. R. 1993, ApJS, 86, 517
Zickgraf, F. J., Humphreys, R. M., Sitko, M. L., & Manley, T. 1990, PASP, 102, 925